Correspondence to:
Y.-S. Choi,
ysc@ewha.ac.kr

Revisiting the iris effect of tropical cirrus clouds with TRMM and A-Train satellite data

Yong-Sang Choi[1,2] (iD), WonMoo Kim[3] (iD), Sang-Wook Yeh[4] (iD), Hirohiko Masunaga[5] (iD), Min-Jae Kwon[6] (iD), Hyun-Su Jo[7], and Lei Huang[2,8]

[1]Department of Environmental Science and Engineering, Ewha Womans University, Seoul, South Korea, [2]NASA Jet Propulsion Laboratory, California Institute of Technology, Pasadena, California, USA, [3]Climate Prediction Department, APEC Climate Center, Busan, South Korea, [4]Marine Sciences and Convergent Technology, Hanyang University, Seoul, South Korea, [5]Institute for Space-Earth Environmental Research, Nagoya University, Nagoya, Japan, [6]Department of Atmospheric Science and Engineering, Ewha Womans University, Seoul, South Korea, [7]CSIRO Oceans and Atmosphere, Aspendale, Victoria, Australia, [8]Joint Institute for Regional Earth System Science and Engineering, University of California, Los Angeles, California, USA

Abstract Just as the iris of human eye controls the light influx (iris effect), tropical anvil cirrus clouds may regulate the Earth's surface warming by controlling outgoing longwave radiation. This study examines this possible effect with monthly satellite observations such as Tropical Rainfall Measuring Mission (TRMM) precipitation, Moderate Resolution Imaging Spectroradiometer cirrus fraction, and Clouds and the Earth's Radiant Energy System top-of-the-atmosphere radiative fluxes averaged over different tropical domains from March 2000 to October 2014. To confirm that high-level cirrus is relevant to this study, Cloud-Aerosol Lidar with Orthogonal Polarization high cloud observations were also analyzed from June 2006 to December 2015. Our analysis revealed that the increase in sea surface temperature in the tropical western Pacific tends to concentrate convective cloud systems. This concentration effect very likely induces the significant reduction of both stratiform rain rate and cirrus fraction, without appreciable change in the convective rain rate. This reduction of stratiform rain rate and cirrus fraction cannot be found over its subregion or the tropical eastern Pacific, where the concentration effect of anvil cirrus is weak. Consistently, over the tropical western Pacific, the higher ratio of convective rain rate to total rain rate (i.e., precipitation efficiency) significantly correlates with warmer sea surface temperature and lower cirrus fraction. The reduced cirrus eventually increased outgoing longwave radiation to a greater degree than absorbed solar radiation. Finally, the negative relationship between precipitation efficiency and cirrus fraction tends to correspond to a low global equilibrium climate sensitivity in the models in the Coupled Model Intercomparison Project Phase 5. This suggests that tropical anvil cirrus clouds exert a negative climate feedback in strong association with precipitation efficiency.

Plain Language Summary The Earth may have a cooling mechanism, so called the iris effect, under green house gas forcing, as if human eyes control the light influx. This feedback process of the tropical cloud to increased sea surface temperature is confirmed using various satellite observation. It is found that the precipitation efficiency increases as the temperature increases and the cirrus decreases as the precipitation efficiency increases in the tropical Western Pacific. This negative relationship suggests the presence of the cooling mechanism (negative feedback). Our climate models also tend to show lower warming rate if the observed negative relationship is properly mimicked, vice versa.

1. Introduction

Clouds are the most powerful radiative substances in the Earth's atmosphere. They can control global outgoing and incoming energy fluxes. It is known that the climate sensitivity (or the climate scenario for given increasing greenhouse gases) is directly associated with the clouds. Current climate models show a large diversity in climate sensitivity estimates, especially due to our lack of understanding of clouds [*Stocker et al.*, 2013]. Different climate sensitivity estimates in current climate models are mainly attributed to highly uncertain cloud feedbacks [*Bony et al.*, 2015; *Sherwood et al.*, 2014; *Zelinka and Hartmann*, 2010]. However, a limited capacity to observe clouds veils that clouds play the multiple roles in the climate feedbacks [*Choi et al.*, 2005; *Ohring et al.*, 2005].

Clouds react to sea surface temperature (SST) change, especially in the tropical warm pool region. High SSTs over 27°C can typically invigorate deep convective clouds and thereby affect upper tropospheric anvil cirrus

clouds [*Graham and Barnett*, 1987; *Sud et al.*, 1999; *Kubar et al.*, 2011; *Behrangi et al.*, 2012]. This cloud reaction in turn changes SST usually within a few days; that is, clouds alter as well as respond to SST [*Waliser and Graham*, 1993]. The present question is if this tropical cloud feedback process is vitally important in climate sensitivity.

Several different processes of tropical cloud feedbacks to SST have been suggested [*Hartmann and Larson*, 2002; *Horváth and Soden*, 2008; *Ramanathan and Collins*, 1991; *Rondanelli and Lindzen*, 2008; *Wood*, 2007]. The suggested cloud feedbacks, though they can be valid individually, cannot account for the observed total longwave energy reaction to SST in the tropics. Several observational studies clearly show that at least tropical outgoing longwave radiation (OLR) anomalies strongly increase with increasing SST anomalies [*Cho et al.*, 2012; *Lindzen and Choi*, 2011; *Mauritsen and Stevens*, 2015] by about 4 to 6 W m^{-2} K^{-1}. This is indeed far above the Planck response to increasing SST, which would not be achieved if any type of clouds increased with increasing SST. In other words, these OLR analysis results, in fact, entirely imply the possibility of negative longwave cloud feedbacks.

Lindzen et al. [2001] suggested that a longwave effect of anvil cirrus clouds would act as a negative feedback. This is the so-called Iris effect, where clouds behave like the iris in the human eye, controlling the incoming light. It is based on signals from geostationary satellites showing daily radiances where cirrus clouds decrease with increasing SST. Subsequent studies using other data and methodologies have found supporting results [*Rondanelli and Lindzen*, 2008, 2010a, 2010b]. A slower hydrological cycle was presented in a radiative-convective simulation of the iris effect in *Rondanelli and Lindzen* [2010a]. Likewise, a recent paper by *Mauritsen and Stevens* [2015] showed that implementing the iris effect in climate models improves simulation of the global hydrological cycle, and global OLR and lapse rate responses, to changing SST.

In fact, this iris effect was tested in several aspects. First, *Hartmann and Michelsen* [2002a] argued that the cirrus was from the subtropics, not from the tropical convective system. Their assertion was primarily grounded by the correlation analysis between cloud amount for "each grid" and cloud-weighted SST averaged "over the whole domain." *Lindzen et al.* [2002] responded that such an analysis is not appropriate to test the iris effect since it cannot capture clouds popping up in different locations over the tropical western Pacific and moving to the next grid. Second, a net radiative effect of anvil cirrus clouds was questioned [*Fu et al.*, 2002; *Lin et al.*, 2002]. *Mauritsen and Stevens* [2015] also show that the shortwave effect of cirrus clouds still provides a net positive feedback in their model. With respect to this, *Choi and Ho* [2006] showed that on the contrary, most tropical cirrus clouds have a stronger longwave effect than a shortwave effect in direct observations from a satellite. Nevertheless, this study will resolve this issue by directly showing both longwave and shortwave radiative fluxes in relation to cirrus fraction. Other criticisms were about discrepancies in the cloudy moist area between *Lindzen et al.* [2001] and the analyses by others [*Chambers et al.*, 2002; *Lin et al.*, 2004, 2006; *Rapp et al.*, 2005; *Su et al.*, 2008]. The detailed replies to those criticisms can be found in *Chou et al.* [2002a, 2002b; *Chou and Lindzen*, 2002], *Chou and Lindzen* [2005], and *Rondanelli and Lindzen* [2010b].

Rondanelli and Lindzen [2010b] pointed out several methodology cautions when using satellite data to study the iris effect. They include classifying cloudy regions into convective updrafts and anvils, using cloud-weighted SST, and truncating and sampling errors of orbital satellite data. By careful consideration of these earlier points, this study inquires whether the iris effect of tropical anvil cirrus clouds plays a significant role in global climate sensitivity.

2. Data and Methods

We used monthly cloud fraction, radiative fluxes, SSTs, and rainfall rates from different sources. The analysis period is from March 2000 to October 2014, during which all the following satellite retrievals are available (Terra was launched in March 2000, and the Tropical Rainfall Measuring Mission (TRMM) data were available until October 2014). First, the cloud fraction is estimated from the Moderate Resolution Imaging Spectroradiometer (MODIS)/Terra by the National Aeronautics and Space Administration (NASA) (MOD08_M3 version 6 for 1° monthly data and MOD08_D3 version 6 for daily data). The MODIS clouds from different retrieval methods have different optical depth coverages. We used the MODIS cirrus fraction with 1.38 μm reflectivity (SWIR) (greater than optical depth of ~0.1) [*Choi et al.*, 2005] (hereafter, CiF). This MODIS cirrus fraction covers most of the high clouds above 500 hPa and is approximately twice of Geostationary Meteorological Satellite-5 (GMS) high clouds determined by 11–14 μm brightness temperatures (<260 K) used in *Lindzen et al.* [2001] and [*Choi et al.*, 2005]. Moreover, this MODIS cirrus cloud

fraction covers all high clouds including cumulonimbus and often overlaying low clouds [*Choi and Ho*, 2006]. Accordingly, there is no upper cutoff of optical depth in the MODIS cirrus cloud fraction.

This MODIS cirrus fraction limitation was overcome using vertical cloud retrievals from the Cloud-Aerosol Lidar with Orthogonal Polarization (CALIOP), which is a dual wavelength polarization lidar designed to acquire vertical profiles of attenuated backscatter from a near nadir-viewing geometry during both day and night phases [*Winker et al.*, 2007]. It is one member of the A-Train [*L'Ecuyer and Jiang*, 2010] satellite constellation and has been continuously collecting high-resolution (1/3 km in the horizontal and 30 m in the vertical below 8.3 km, and 1 km in the horizontal and 60 m in the vertical for the higher altitudes of 8.3–20.2 km) profiles of the attenuated backscatter by aerosols and clouds at 532 nm and 1064 nm wavelengths along with polarized backscatter at 532 nm between 82°N and 82°S [*Winker et al.*, 2007]. The sensor is known to be particularly sensitive to high cirrus clouds. The features identified by CALIOP are first classified into aerosol and cloud using a cloud-aerosol discrimination (CAD) algorithm [*Liu et al.*, 2009]. The level of confidence in the aerosol-cloud classification is reflected by a CAD score, with negative values (−100–0) for aerosol and positive values (+100–0) for cloud. In this study, we used the CALIOP Version 3 Level 2 cloud profile data (CAL_LID_L2_05kmCPro), which are reported at a uniform spatial resolution of 60 m vertically and 5 km horizontally, over a nominal altitude range from 20 km to −0.5 km. By accumulating the pixel data from June 2006 to December 2015, we generated monthly 5° longitude × 4° latitude gridded cloud frequency data to ensure there was a sufficient number of samples in each grid box.

The radiative flux at the top of the atmosphere (TOA) is from the Clouds and the Earth's Radiant Energy System (CERES)/Terra by NASA (the ES4 Terra-Xtrk Edition 3 product for 2.5° monthly data available at https://eosweb.larc.nasa.gov/project/ceres/ceres_table) [*Wielicki et al.*, 1996]. We used TOA absorbed shortwave radiation (ASR) and outgoing longwave radiation (OLR). The ASR was calculated by subtracting reflected shortwave radiation from incident shortwave radiation. ASR minus OLR therefore determine the net energy gain in the Earth-atmosphere system. The uncertainties of the SW and LW radiations at TOA directly measured by the CERES are ~5% and ~1%, respectively [*CERES Science Team*, 2013].

The SST is from the National Oceanic and Atmospheric Administration (NOAA) (the optimal interpolated SST version 2 0.25° data). Relating the aforementioned monthly cloud, rainfall, and radiative flux data necessarily requires monthly averaging of the daily SSTs. However, monthly averaging is also needed for other reasons. In all domains of this study (section 3), the land surface temperature was not considered due to its excessively fast response to many factors. Whether land surface temperature was included or excluded, the usual coefficient of determination between daily cloud and SST becomes very low ($r^2 = 0.05$). In order to resolve this unclear cloud-SST relationship, in *Lindzen et al.* [2001], SST was weighted by cloud area (< 260 K) since clouds are not affected by SST for the whole domain but by SST under cloud layers. However, this cloud weighing can amplify random cloud effects that change SST [*Hartmann and Michelsen*, 2002b; *Cho et al.*, 2012]. Furthermore, clouds may not only be affected by SSTs under cloud layers. SST gradients away from clouds can drive local circulations and cloud development as well. This study is therefore based on "monthly" averaged SST data over the domains to minimize locally varying SST by cloud forcing. "Daily" SST has more local variation. Note that the monthly averaged SST also avoids the sampling problem from the Sun-synchronizing satellites.

The rain rate is from the TRMM by NASA and Japan Aerospace Exploration Agency (3A25 version 7 for 0.5° monthly data). The TRMM rainfall rate has three types: total, convective, and stratiform rainfall rates (in mm h^{-1}). The TRMM 3A25 provides monthly mean rainfall from precipitation radar (PR) measurements. The TRMM PR selectively detects precipitating particles with little sensitivity to smaller, nonprecipitating cloud droplets and ice crystals. As such, convective and stratiform rain are measured independently of cirrus clouds from MODIS, which contain a much broader area of high clouds regardless of precipitation beneath the clouds. The distinction between convective and stratiform rainfall is determined based on the existence of bright band (BB) and the reflectivity change near the BB height [*Awaka et al.*, 2007]. The domain-averaged convective rain (CR) and stratiform rain (SR) are calculated as

$$CR = \frac{\sum_i \left(R_{c,i} \, N_{c,i}/N_{obs,i} \right) \cos\theta_i}{\sum_i \cos\theta_i} \tag{1a}$$

$$SR = \frac{\sum_i \left(R_{s,i} \, N_{s,i}/N_{obs,i} \right) \cos\theta_i}{\sum_i \cos\theta_i} \tag{1b}$$

where i is the ith grid of the domain and θ is the latitude. The subscripts c, s, and obs, represent the convective rain, stratiform rain, and total observed pixels, respectively. R is the rainfall rate (mm h^{-1}), and N is the number of pixels. R should be weighted by N since R per se is only the average over the rainy pixels and does not include the other observed pixels in a grid. The CR and SR are hereafter displayed in mm/d (mm d^{-1}) since the area-averaged values in mm h^{-1} are too small. All rainfall data were obtained from TRMM observations.

The constraint of anvil cirrus clouds may be subject to the distribution of the two types of rain; stratiform rain originates from the anvil clouds, while convective rain from convective cloud cores. Convective rain is much stronger (more precipitation in a given time) than stratiform rain. Therefore, the overall precipitation efficiency of the convective cloud system is determined by the ratio of the two types of rain [*Rondanelli and Lindzen*, 2008], convective and stratiform rain. From TRMM data available in this study, the convective rain fraction-based precipitation efficiency (PE) is defined as the convective rain rate normalized by the total rain rate:

$$PE = \frac{CR}{CR + SR} \qquad (2)$$

By the definition 2, a higher PE means that more moisture is allotted to convective rain than stratiform rain. Note that this is different from the traditional concept of precipitation efficiency defined in terms of the ratio of precipitation to surface moisture convergence [*Sui et al.*, 2007, and references therein], which refers to the combined effects of dynamics and cloud microphysics in producing rainfall. However, the greater ratio of CR to total rain in equation 2 is eventually associated with the higher precipitation efficiency defined traditionally.

Finally, we also applied the same methodology to the Coupled Model Intercomparison Project Phase 5 (CMIP5) (i.e., twentieth century runs for the same period as in this study). Only 22 models whose outputs include SST, precipitation flux and convective precipitation flux, CiF, and OLR together are shown in this study. Among these models, only 13 models have documented equilibrium climate sensitivity (ECS) [*Sherwood et al.*, 2014]. The ECS is effective climate sensitivity calculated from abrupt $4 \times CO_2$ experiments following a standard regression procedure between TOA radiance and surface temperature [*Sherwood et al.*, 2014]. In these models, the precipitation efficiency is defined as the convective precipitation flux (kg m^{-2} s^{-1}) divided by the total precipitation flux (kg m^{-2} s^{-1}). CiF is substituted for cloud area fraction in the atmospheric layers, 0.1 and 0.2 hybrid sigma pressure levels. Our analyses are based on these top-level cloud layers in the models since our interest is their strong longwave warming effect and their different behaviors in changing outgoing longwave radiation. However, these cloud fractions in the models cannot be directly compared with MODIS CiF since the modeled outputs do not clearly identify the actual total fraction of overlapping multilayer clouds like MODIS.

3. Observed Behaviors of Tropical Cirrus and Precipitation

The key mechanism behind the iris effect lies in the cloud-precipitation relationship wherein precipitation constrains the cloud system. *Mauritsen and Stevens* [2015] dealt with cloud-to-precipitation conversion rate in their climate model for identifying the iris effect, but the cloud-precipitation relationship determining the conversion rate remains largely uncertain in the observations.

Moreover, the choice of the domain requires careful consideration of cirrus cloud behavior. Cloud clusters are aggregated to a warmer SST in TWP [*Lindzen et al.*, 2001; *Mauritsen and Stevens*, 2015]. So if the domain is too large, cloud clusters intrude into the domain from outside. Also, if the domain is too small, it cannot cover (or can miss) movement of cloud clusters or the entire fraction of cirrus anvils. Therefore, the domain needs to cover an area large enough to track cloud clusters over a distance, but small enough to avoid exterior clouds. Several choices in the tropics were tested as research domains for this study. A high fraction of tropical cirrus clouds is widely distributed over the tropical western Pacific [*Choi and Ho*, 2006] (TWP [120°E–155°W, 30°S–30°N]) (Figure 1a). Over the TWP, clouds commonly react fast to the SST changes [*Graham and Barnett*, 1987; *Zhang*, 1993; *Sud et al.*, 1999; *Kubar et al.*, 2011; *Behrangi et al.*, 2012]. Thereby, TWP has been popularly chosen to study cloud feedback [*Choi and Ho*, 2006; *Lindzen et al.*, 2001]. We also confined our analysis to the subregion of the TWP, the Pacific warm pool (PWP [130°E–170°W, 20°S–20°N]) where the land surface and subtropical Hadley subsidence are excluded, following previous studies [*Horváth and Soden*, 2008; *Ramanathan and Collins*, 1991; *Rondanelli and Lindzen*, 2008].
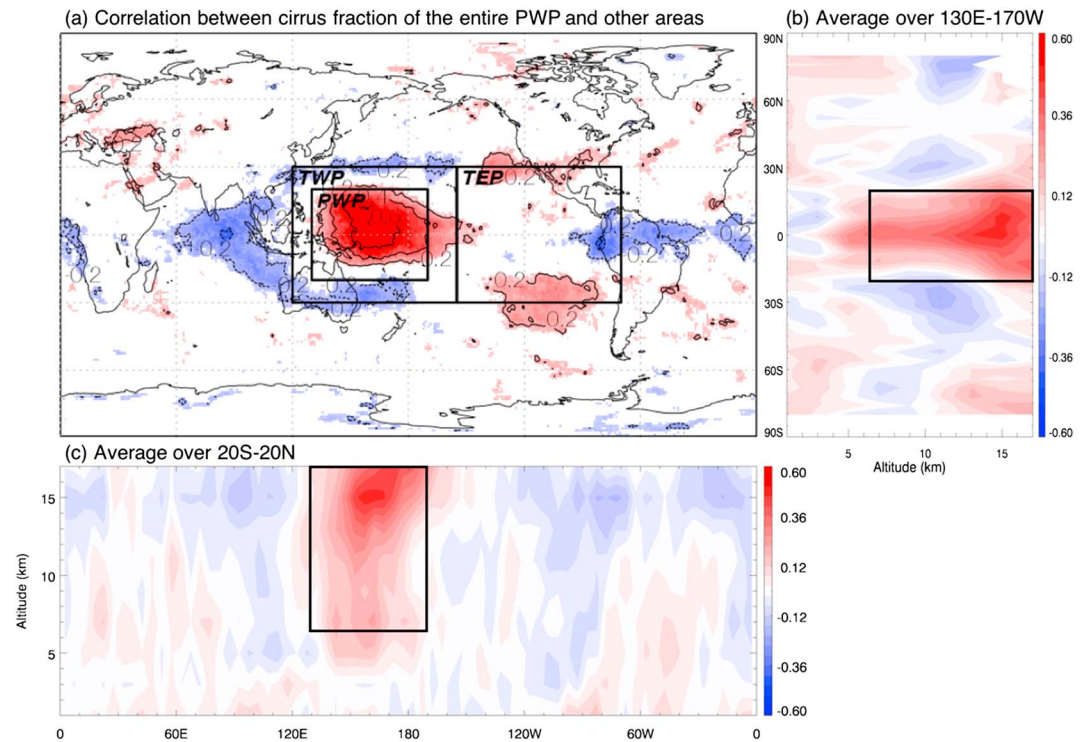
Figure 1. (a) Correlation between the time series of monthly MODIS cirrus fraction of the entire PWP region and that of the 1° grid boxes over the globe. The TWP, PWP, and TEP regions are indicated as boxes. Only significant correlation at 95% confidence level is shaded in colors. (b) The meridional region (130°E–170°W), and (c) the zonal region (20°S–20°N) averaged correlations between the time series of CALIOP cloud fraction of all the levels (0–17 km) and that integrated above 6.5 km (~440 hPa) in the PWP region. The results in Figures 1b and 1c are calculated from CALIOP observations from June 2006 to December 2015.

Over the tropical eastern Pacific (TEP [155°W–70°W, 30°S–30°N]), clouds do not respond well to the SST changes. There is the asymmetry of the near equatorial Pacific, with cool SSTs and subsidence prevalent year-round in the southeastern Pacific, which is included in the TEP. On the other hand, the TWP is very warm and convectively active. Thereby, it is known that the cirrus fraction over the TWP is much larger than over the TEP [*Choi and Ho*, 2006; *Kubar et al.*, 2007]. Likewise, we will see that the warmer PWP region, a subregion of the TWP, has more cirrus clouds than the TWP in general. Therefore, we selected the TEP to be referenced as a cold region far from the TWP. The TEP is better than a smaller eastern Pacific domain for this study to avoid the effect of a seasonal change in the Intertropical Convergence Zone (ITCZ) and to compare with the results from the other similar-sized domains, TWP or PWP. We note that all the relationships shown hereafter (of CiF-CR, CiF-SR, CiF-PE, and CiF-SST) over a part of the ITCZ [110°W–170°W, 4°N–10°N] were found to be the opposite to those of the TWP. Therefore, this shows an important compensating subsidence away from the center of anomalous convection when examining the iris effect.

The cloud-precipitation relationship should reflect the concentration of several deep convective clouds (DCCs) on the domains. This is directly supported by our spatial correlation analysis clearly showing that monthly MODIS cirrus fraction over the PWP, a subregion of the TWP, varies inversely with that over the surroundings (Figure 1a). Quantitatively, the correlation coefficient (r) between the area-averaged cirrus fraction over the PWP and that over the surrounding region outside the PWP (but inside the TWP) is −0.44. This negative correlation is confined to the tropics within about 30°S to 30°N. It is also broadly distributed over the Indian Ocean. On the other hand, the MODIS cirrus clouds used in Figure 1a include all high clouds with tops above 500 hPa but may not distinguish a single-layer cirrus from cirrus overlaying low-level clouds or cumulonimbus towers. It is possible to clarify the cloud type issue with CALIOP cloud data that are vertically resolved and sensitive to cirrus clouds. Our additional analysis with CALIOP cloud data (June 2006 to December 2015) reconfirms that this negative correlation is relevant to high cirrus clouds (Figures 1b and 1c). It shows that the decrease in tropical cirrus clouds outside the PWP, with increasing clouds over the PWP, is
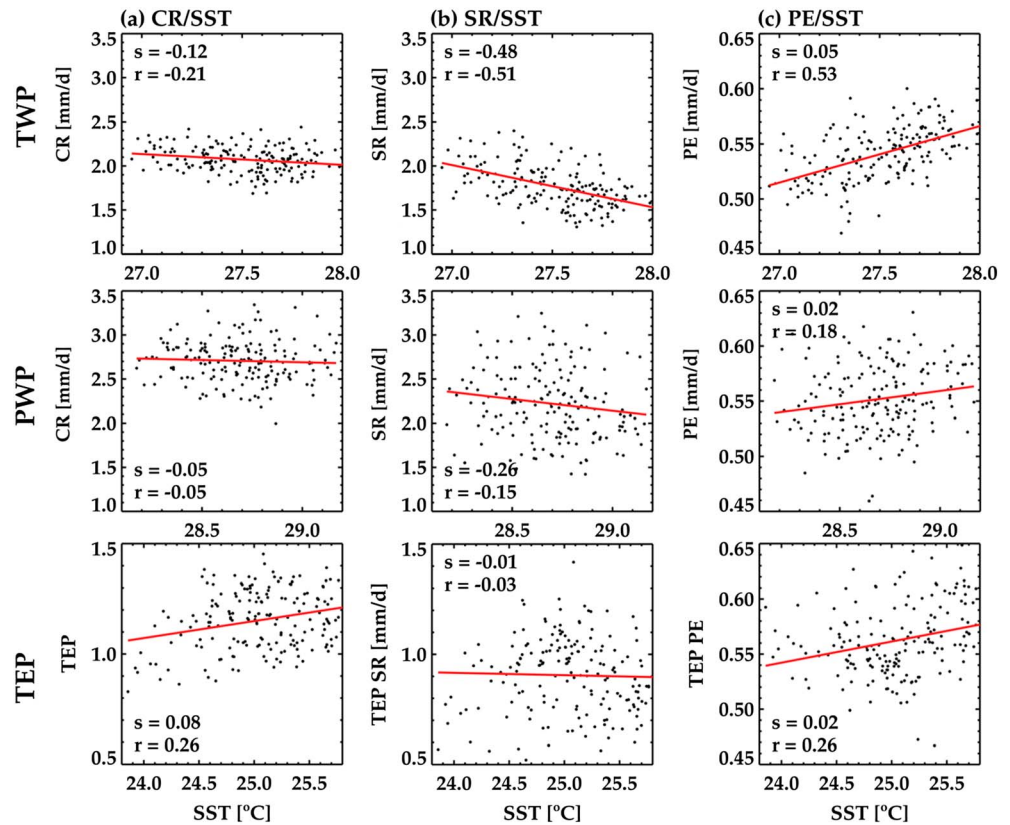
Figure 2. SST against (a) CR in mm d^{-1}, (b) SR in mm d^{-1}, and (c) PE over TWP, PWP, and TEP. *s* indicates the regression slope, and *r* indicates the correlation coefficient.

clear particularly between 10 km and 16 km. However, this figure indicates neither the iris effect of a single convective cloud nor the self-aggregation of several convective clouds [*Muller and Bony*, 2015]. Rather, it may represent a large-scale analogy of the aggregation effect whose mechanism relies more upon the large-scale dynamics [*Bony et al.*, 2016]. That is to say, when the ascent anomaly inside the PWP increases, it forces the descent anomaly in adjacent areas, leading to the reduced convection and cirrus fraction outside the PWP.

Consequently, many cirrus anvil layers from different convective cores can overlap and are constrained by moisture converged into the system. In other words, a doubling of tropical convective cloud systems would not double anvil cirrus fraction and precipitation. A cloud feedback process should involve this constraint efficiency.

To embrace this constraint efficiency, the TWP may be more appropriate than PWP (a subregion of TWP). Figure 2 shows SST-CR, SST-SR, and SST-PE relationships for each domain. The plots designate the domain-averaged monthly SST and precipitation values by equations 1a, 1b, and 2. First of all, more DCCs were typically expected for higher SST, but the CR is not so dependent on SST regardless of the domain (Figure 2a). This is likely because CR also originates from shallow convective clouds under a lower SST. Overall, the SST-SR or SST-PE relationship becomes stronger with the expansion of the domain from the PWP to the TWP. It implies that these relations are largely manifested by large-scale dynamical effects such that the area between the TWP and the PWP borders undergoes atmospheric subsidence in response to the deep convection over the PWP.

In Figure 2b (top), the SR tends to decrease with increasing SST over the TWP. The decreasing rate of SR per SST is approximately −0.48 mm d^{-1} K^{-1} over TWP ($r = -0.51$). The rate and correlation persist for lagged SSTs from the next month to SR but disappear completely for leading SSTs from 1 month in advance of SR (not shown). Moreover, the PWP SST is weakly related to any type of precipitation, such that colder SSTs in between the PWP and TWP may be affected by cloud variations [*Hartmann and Michelsen*, 2002a;

Su et al., 2008]. In the physical relationship of monthly variables, the atmospheric radiative forcings more directly affect SST tendency (the difference between the two consecutive months) than SST itself [*Choi et al.*, 2014]. Therefore, the relationship between SST tendency and SR is also discussed here. The relationship between SST tendency and SR in the preceding month turns out to be almost entirely trivial ($r = -0.1$) over the TWP, but significant ($r = -0.4$) over the TEP (not shown). This means that the cloud cooling effect on SST is significant over the TEP while not over TWP. The latter result with SST tendency is seemingly contradictory to the former result with SST. This may result from the fact that clouds and SST interact with each other. The cloud cooling effect on SST more clearly appears on a shorter time scale (hours to days); however, on a monthly scale, it is rather more clearly observed convective activities responding to the SSTs warmer than about 27°C. Consequently, the negative SST-SR relationship in the TWP (Figure 2b, top) can arise from not only the cloud cooling effect on SST (that is dominant outside the PWP) but also the cloud response to SST (that is dominant inside the PWP).

Over the PWP, the SST-SR and SST-PE relationships are very weak (Figures 2b (middle) and 2c (middle)). This means that the entire cloud/precipitation responding to SST may not be captured over PWP but escapes out over a larger area, the TWP. The influence of the large-scale climate variability like El Niño–Southern Oscillation (ENSO), Madden-Julian Oscillation, and Tropospheric Biennial Oscillation is not likely affecting the relationships in Figure 2, since SST-SR or SST-PE over the PWP is fairly different from those over the TWP. This apparent difference in the results between the TWP and PWP indicates how sensitive the results are to the choice of the domain.

It is known that a convective core occupies a much smaller area than a stratiform cirrus ($<1/100$) [*Choi and Ho*, 2006]; however, CR originating in the convective core is larger than SR from a cirrus area. This means that precipitation cannot just be weighted by cloud fraction but should be scaled by the total mass influx into the convective cloud system [*Choi and Ho*, 2006]. This is why we need to look further into PE. Consequently, the SST-PE relationship appears to be positive over the TWP ($r = 0.53$), which is more apparent than in the PWP ($r = 0.18$). The PE/SST was found at a rate about 5% K^{-1} over the TWP and less over the PWP or TEP. This positive SST-PE relation over the TWP is also shown in *Rondanelli and Lindzen* [2008] (6–12% K^{-1}) which is based on 2° grid monthly variables for the year 2001. Their study reflects more spatial variation within the TWP and allows a wider SST range from 16°C to 33°C, while the present study reflects more temporal variation of the domain averages. Over the PWP and TEP, none of the precipitation types were clearly related to SST (Figure 2, middle and bottom).

We then examined precipitation-CiF relationships for each domain (Figure 3). The MODIS cirrus fraction and TRMM precipitation retrievals used in this analysis are from independent satellite algorithms, so their relationship would not be an artifact. CiF over both the TWP and PWP has a strong positive relationship with CR. The concentration effect of DCCs on the domains, as shown above, may somewhat differentiate CR-CiF relations between the TWP and PWP (Figure 3a, top and middle). On the other hand, CiF over both the TWP and PWP has a clear positive relationship with SR, while such is hardly realized in the TEP (Figure 3b). CiF may not be constrained by any type of precipitation over the TEP. In accordance with the relationship in Figure 3b, CiF has a strong negative relation with PE over the TWP and PWP (Figure 3c).

The negative PE-CiF (Figure 3c) is intriguing because this is consistent with the expectation based on the iris mechanism [*Lindzen et al.*, 2001]. In the iris mechanism [*Lindzen et al.*, 2001], if more rain falls out from the convective core of DCCs, there remains less moisture at the upper level cloud core per total mass flux into the system. The reduced moisture may induce the reduction of stratiform precipitation as well as anvil cloud fraction. Based on this mechanism, the anvil cirrus fraction is expected to be in a close relationship to SR, but not so to CR, and therefore inversely proportional to PE. Such a difference between the CR-CiF and SR-CiF correlations is more distinctive over the TWP than the PWP.

One may suppose that the PE-CiF relationship is always negative as just a mathematical artifact, because the denominator of equation 2 calculating PE contains SR that was found to increase with increasing CiF (Figure 3b). However, the regression slope (and correlation) of CiF/PE (Figure 3c) can vary greatly with the CR-SR relationship, which should retain physical meaning. If SR is linearly proportional to CR, PE will be nearly constant (by equation 2) regardless of the CiF. This case is inconsistent with the negative PE-CiF relationship over the TWP (Figure 3c, top). Over the TEP, CiF is hardly related to PE (Figure 3c, bottom). Apparently, the negative CiF-PE relationship occurs when SR is inversely proportional to CR or independent of CR (i.e., SR per given
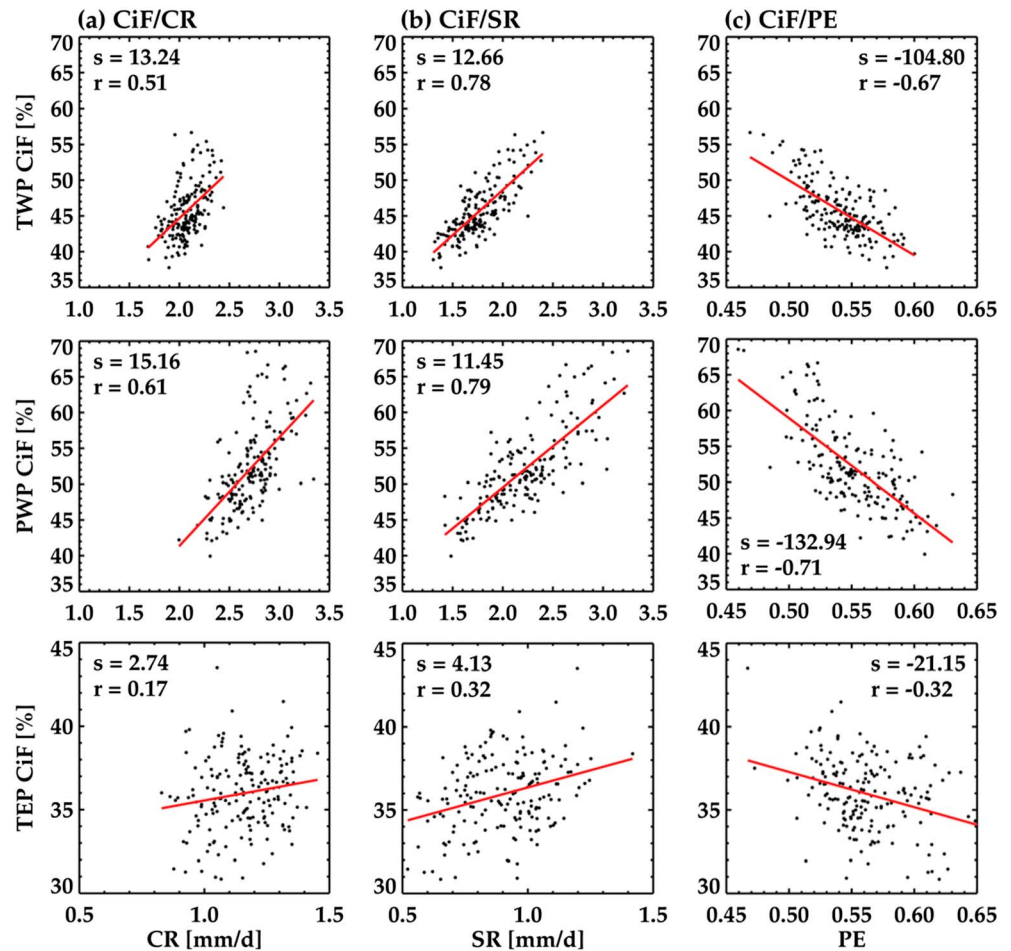
Figure 3. (a) CR, (b) SR, and (c) PE against CiF over TWP, PWP, and TEP. Note the different scales.

mass influx decreases with increasing convective strength). Our observations show that the latter corresponds to the actual situation over the TWP (Figure 3c, top).

The above slopes and correlations in Figures 2 and 3 do not change much when only taking the area-averaged variables for each season. This means that the relationships do not just come from the annual cycle. The detailed seasonal results are shown in Table 1.

Figure 4 shows the combination of Figures 2 and 3. It implies a mechanism in cloud feedback to SST. Over the TWP, less CiF seems to be constrained by higher PE in association with warmer SST (Figures 2c (top) and 3c (top), and 4a). Although the constraint of CiF by PE is somewhat evident, the influence of SST is unclear over the PWP (Figures 2c (middle) and 3c(middle), and 4b). Over the TEP, these are entirely unclear (Figures 2c (bottom) and 3c (bottom), and 4c). The TEP is widely known as a large-scale subsidence region where SST is relatively low and uncoupled with convective cloud systems. Thus, the anvil cirrus there is seldom participating in cloud feedback. These results indicate that the connection between cirrus, precipitation, and SST is region dependent, which may have caused very different conclusions concerning cloud feedback to SST in previous studies. In summary, the cloud feedback concerning CiF is sound only over TWP.

4. Radiative Effect of Tropical Cirrus and Equilibrium Climate Sensitivity

Quantitatively, the 1% reduction in CiF corresponds to the increase in OLR of ~0.7 W m^{-2} (Figure 5a, top) and the increase in ASR of ~0.3 W m^{-2} over the TWP (Figure 5b, top). The OLR dominates over ASR in the total radiative flux at TOA (Figure 5c). ASR fluctuates to a large extent by the annual cycle (clusters in Figure 5b), but the increasing rate of ASR per CiF is cleaner (and somewhat higher) when confining the plots to a

Table 1. The Regression Slopes and Correlations for the Area-Averaged Variables for DJF (December–February Period), MAM (March–May Period), JJA (June–August Period), and SON (September–November Period). CR/SST and SR/SST in mm d^{-1} K^{-1}, and PE/SST in K^{-1} (Figure 2); CiF/CR, and CiF/SR in % mm^{-1} d Figure 3; CiF/PE in %; and OLR/CiF, ASR/CiF, and (ASR–OLR)/CiF in W m^{-2} %$^{-1}$ (Figure 5)[a]

Domains		TWP (12,024°E–155°W, 30°S–30°N)		PWP (130°E–170°W, 20°S–20°N)		TEP (15,524°W–70°W, 30°S–30°N)	
Seasonal Relations		Slope	Correlations	Slope	Correlations	Slope	Correlations
CR/SST	DJF	−0.07	−0.10	0.04	0.04	**0.09**	**0.46**
	MAM	**−0.52**	**−0.69**	**−0.57**	**−0.47**	0.06	0.10
	JJA	−0.21	−0.22	−0.22	−0.18	0.09	0.31
	SON	−0.05	−0.07	0.10	0.11	**0.22**	**0.65**
SR/SST	DJF	**−0.42**	**−0.40**	−0.35	−0.18	**0.14**	**0.36**
	MAM	**−0.62**	**−0.60**	−0.48	−0.24	0.06	0.09
	JJA	−0.37	−0.27	−0.51	−0.25	0.05	0.12
	SON	−0.24	−0.21	−0.03	−0.02	**0.23**	**0.58**
PE/SST	DJF	**0.05**	**0.46**	0.04	0.29	−0.02	−0.20
	MAM	0.02	0.24	0.00	0.00	−0.01	−0.06
	JJA	0.03	0.19	0.04	0.26	0.01	0.12
	SON	0.03	0.21	0.01	0.08	−0.01	−0.26
CiF/CR	DJF	**7.61**	**0.32**	**14.88**	**0.56**	6.20	0.18
	MAM	**11.90**	**0.65**	**14.33**	**0.64**	**6.52**	**0.33**
	JJA	**9.17**	**0.56**	**10.86**	**0.68**	4.14	0.23
	SON	**13.62**	**0.61**	**13.54**	**0.68**	3.62	0.24
CiF/SR	DJF	**10.44**	**0.73**	**12.33**	**0.85**	**11.45**	**0.66**
	MAM	**10.65**	**0.79**	**11.02**	**0.81**	**6.25**	**0.37**
	JJA	**7.33**	**0.66**	**7.67**	**0.79**	**8.52**	**0.60**
	SON	**9.38**	**0.66**	**8.72**	**0.75**	**4.23**	**0.33**
CiF/PE	DJF	**−101.56**	**−0.70**	**−150.59**	**−0.80**	**−43.75**	**−0.66**
	MAM	**−75.23**	**−0.53**	**−130.00**	**−0.71**	−16.74	−0.24
	JJA	**−49.57**	**−0.47**	**−87.13**	**−0.69**	**−37.72**	**−0.53**
	SON	**−64.61**	**−0.50**	**−104.28**	**−0.69**	**−30.25**	**−0.31**
OLR/CiF	DJF	**−0.89**	**−0.89**	**−1.04**	**−0.97**	**−0.65**	**−0.72**
	MAM	**−0.82**	**−0.84**	**−0.88**	**−0.94**	**−0.77**	**−0.78**
	JJA	**−0.91**	**−0.92**	**−1.07**	**−0.96**	**−0.52**	**−0.63**
	SON	**−0.77**	**−0.84**	**−0.92**	**−0.92**	**−0.68**	**−0.75**
ASR/CiF	DJF	−0.60	−0.29	**−0.66**	**−0.48**	**−2.49**	**−0.61**
	MAM	**1.54**	**0.42**	0.62	0.26	**−2.56**	**−0.36**
	JJA	**−1.29**	**−0.35**	**−0.94**	**−0.40**	−0.10	−0.02
	SON	**−1.80**	**−0.76**	**−1.07**	**−0.70**	**−0.71**	**−0.36**
(ASR–OLR)/CiF	DJF	0.29	0.14	**0.38**	**0.30**	**−1.85**	**−0.49**
	MAM	**2.36**	**0.60**	**1.49**	**0.55**	−1.80	−0.26
	JJA	−0.38	−0.11	0.13	0.06	0.42	0.08
	SON	**−1.03**	**−0.55**	−0.15	−0.12	−0.03	−0.02

[a]Regressions validated to the 95% confidence level were denoted by bold letters.
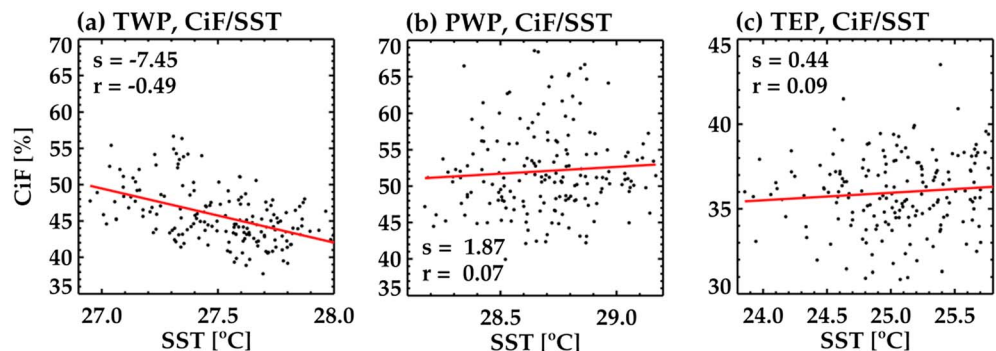
Figure 4. SST against CiF over (a) TWP, (b) PWP, and (c) TEP.
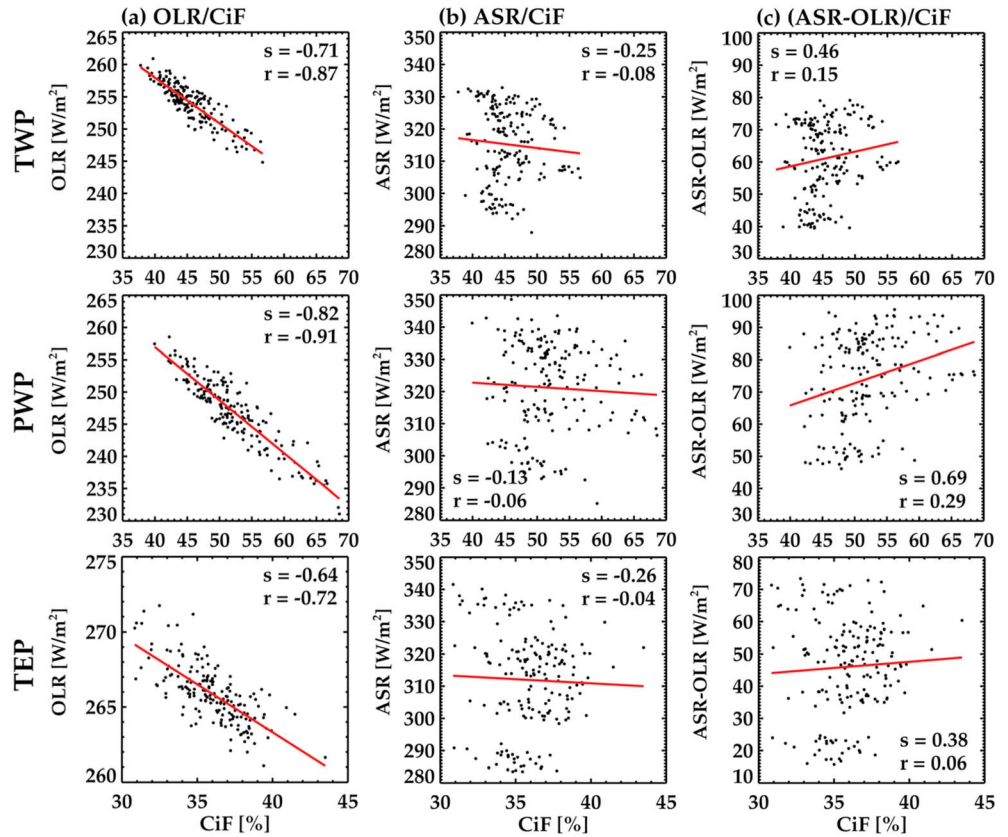
Figure 5. CiF against (a) OLR, (b) ASR, and (c) net radiative flux (ASR minus OLR).

particular season or month (Table 1). This is compatible with the results of *Choi and Ho* [2006] based on a combination of the MODIS MOD08 and CERES ES4 data from March 2000 to June 2005. They documented that the cloud radiative effect of tropical high clouds (mainly cirrus with optical depth < 9) was positive overall. Moreover, cirrus clouds can readily warm the troposphere, simulating radiative-convection equilibrium, even though their thickness is sufficient to induce the negative net radiative effect at TOA [*Liou*, 1986]. Based on the direct regression between the 176 monthly variables (OLR (used in Figure 5a, top) and SST (used in Figure 2, top)), the increasing rate of OLR per SST was calculated to be ~6.2 W m^{-2} K^{-1} over TWP (r = 0.53). While it is not as much as the direct regression slope, this positive SST-OLR relationship can also be estimated by a multiplication of the positive SST-PE relationship (Figure 2c, top), negative PE-CiF relationship (Figure 3c, top), and negative CiF-OLR relationship (Figure 5a, top) (3.7 W m^{-2} K^{-1} = 0.05 · −104.80 · −0.71). This is indeed larger than what is expected by Planck response (~3.3 W m^{-2} K^{-1}) plus a radiative damping of the Planck response by the strong water vapor feedback in the tropics. These results imply the presence of negative cloud feedback through the iris-like behavior of clouds.

We, therefore, questioned if the tropical anvil cirrus can control the global climate sensitivity. To answer this question, we applied the same methodology to the current climate models in CMIP5. The detailed rates and correlations between the variables for the models over the TWP are summarized in Table 2. In our analysis, a majority of models simulate the positive relationship between PE and SST (mean PE/SST = 0.14 K^{-1}). While the definition of PE for these observations may be different from that for the model, the modeled PE/SST values are spread around the observed value of 0.05 K^{-1}. However, it should be noted that the PE-SST correlations in the models are generally feeble (mean r = 0.24), compared to the observations (r = 0.53). The change in the domain-averaged OLR per this CiF of the climate models vary centering on the mean value of −0.34 (at 0.1 sigma level) or −1.39 (at 0.2 sigma level) W m^{-2}%$^{-1}$ (see Table 2). In fact, these values are respectively higher and lower than the observed value of −0.71 W m^{-2}%$^{-1}$ for the TWP.

Table 2. The Variables From 22 CMIP5 Models for TWP Include PE/SST in K^{-1}, CiF/PE in Percent, OLR/CiF in W m^{-2}%$^{-1}$, and Equilibrium Climate Sensitivity (ECS) in Kelvin [*Sherwood et al.*, 2014][a]

Models	PE/SST Slope	PE/SST Correlations	CiF(0.1σ)/PE Slope	CiF(0.1σ)/PE Correlations	CiF(0.2σ)/PE Slope	CiF(0.2σ)/PE Correlations	OLR/CiF(0.1σ) Slope	OLR/CiF(0.1σ) Correlation	OLR/CiF(0.2σ) Slope	OLR/CiF(0.2σ) Correlation	ECS
CanESM2	0.00	−0.06	−8.75	−0.05	0.09	0.001	0.01	0.01	**−1.99**	**−0.85**	3.68
CCSM4	2.09	0.16	−43	−0.42	**−2.27**	**−0.58**	**−0.81**	**−0.67**	**−0.29**	**−0.9**	2.92
CESM1-BGC	0.04	0.23	−44	−0.45	**−20**	**−0.61**	**−0.72**	**−0.67**	**−0.28**	**−0.88**	-
CESM1-CAM5	0.25	0.10	0.00	−0.03	0.1	0.057	−0.16	−0.19	**−0.50**	**−0.27**	-
CMCC-CESM	0.04	0.34	−25	−0.28	5.8	0.102	**−0.34**	**−0.35**	**−0.1**	**−0.69**	-
CMCC-CM	**0.06**	**0.52**	**−32**	**−0.43**	−1	−0.06	**−0.45**	**−0.51**	**−0.16**	**−0.73**	-
CMCC-CMS	**0.04**	**0.36**	**−28**	**−0.37**	**−9**	**−0.19**	**−0.75**	**−0.63**	**−0.15**	**−0.86**	-
CSIRO-Mk3.6.0	**0.03**	**0.35**	−4.50	−0.01	**−10.1**	**−0.16**	−0.06	−0.12	**−2.1**	**−0.83**	3.99
Inmcm4	0.02	0.12	−24.10	−0.49	64.05	0.482	0.71	0.3	**−0.72**	**−0.81**	2.07
IPSL-CM5A-LR	0.03	0.33	4.75	0.05	10.19	0.227	**−0.49**	**−0.49**	**−1.9**	**−0.88**	4.10
IPSL-CM5A-MR	0.07	0.50	7.27	0.11	**11.07**	**0.359**	**−0.79**	**−0.66**	**−2.26**	**−0.86**	-
IPSL-CM5B-LR	**0.02**	**0.24**	−1.91	−0.01	11.3	0.18	**−0.32**	**−0.49**	**−1.44**	**−0.91**	2.59
MIROC5	**0.03**	**0.39**	−13.40	−0.13	2.65	0.071	**−0.59**	**−0.52**	**−2.39**	**−0.77**	2.71
MIROC-ESM	−0.01	−0.07	35.92	0.43	1.392	0.023	0.00	0.00	**−1.45**	**−0.87**	4.65
MIROC-ESM-CHEM	−0.03	−0.16	19.37	0.23	−1.6	−0.02	0.16	0.13	**−1.49**	**−0.86**	-
MPI-ESM-LR	0.01	0.17	−19.50	−0.14	−4.61	−0.07	**−0.39**	**−0.45**	**−1.55**	**−0.83**	3.60
MPI-ESM-MR	0.00	0.00	−19.90	−0.19	−0.4	0	**−0.56**	**−0.47**	**−1.37**	**−0.85**	3.44
MPI-ESM-P	**0.03**	**0.37**	**−25.40**	**−0.22**	**−13.6**	**−0.20**	**−0.54**	**−0.55**	**−1.44**	**−0.84**	3.42
MRI-CGCM3	0.08	0.36	**−14.50**	**−0.61**	−3.48	−0.08	−0.01	0.00	**−2.09**	**−0.89**	2.59
MRI-ESM1	0.11	0.46	**−15.40**	**−0.61**	−4.71	−0.12	−0.05	−0.01	**−2.13**	**−0.89**	-
NorESM1-M	**0.05**	**0.33**	−46.90	−0.28	**−39.8**	**−0.61**	**−0.70**	**−0.67**	**−2.37**	**−0.89**	2.83
NorESM1-ME	0.04	0.30	−36.80	−0.21	**−39.5**	**−0.58**	**−0.72**	**−0.67**	**−2.41**	**−0.88**	3.68
Mean Value	0.14	0.24	−15.26	−0.19	−1.97	−0.08	−0.34	−0.35	−1.39	−0.82	3.3

[a]Regressions validated to the 95% confidence level were denoted by bold letters.

A majority of models reproduce the negative relationship between the PE and CiF at the 0.1 sigma level in the TWP (mean CiF/PE = −15.26%) and at the 0.2 sigma level in the TWP (mean CiF/PE = −1.97%). Although the majority agrees on the negative PE-CiF relationship, even some of the models show positive relationships. The PE/CiF ratio indeed varies with models. It is fairly different from the strong clear negative relationship in the observations ($r = −0.67$ and $−0.71$ for the TWP and PWP, respectively). This implies that our current climate models could be underestimating the negative PE-CiF relationship.

In fact, the simulated PE-CiF relationship over the TWP is significantly correlated with the models' equilibrium climate sensitivity (ECS) (Figure 6). Models that have a stronger negative relationship as in the observations tend to have lower ECS, while the models of highest ECS ($> 3.5°C$) exhibit a neutral or even positive PE-CiF relationship. The strong correlation between CiF/PE ratio and ECS ($r = 0.63$) and between PE-CiF correlation and ECS ($r = 0.80$) suggests that a large share of global climate sensitivity is controlled by the tropical convective system and cloud processes. Therefore, tropical anvil cirrus may suppress global warming via the iris-like mechanism as the precipitation efficiency effectively constrains cirrus clouds in convective cloud systems.

5. Summary and Discussions

Figure 7 summarizes our observational results. The DCCs typically bring upper level anvil cirrus (comprising the widest area of the DCC), stratiform rain (the dotted line) (comprising the partial area of the DCC), and convective rain (the solid line) (taking the limited narrow area of the convective core). The cirrus clouds effectively block outgoing longwave radiation (OLR) from the surface due to their very cold cloud tops. When the DCCs are concentrated into the PWP (the subregion of the TWP) under anomalously high SST, the convective rain per the total rain of DCCs increases (relatively more solid lines than the dotted lines) by overlapping cirrus clouds from different convective cores, thereby allowing more OLR out to space and cooling the surface.

Comparison with modeled cirrus clouds needs some discussion. While a direct comparison between the observed and modeled cirrus cloud fractions may not be warranted, this observed feature in Figure 1 was
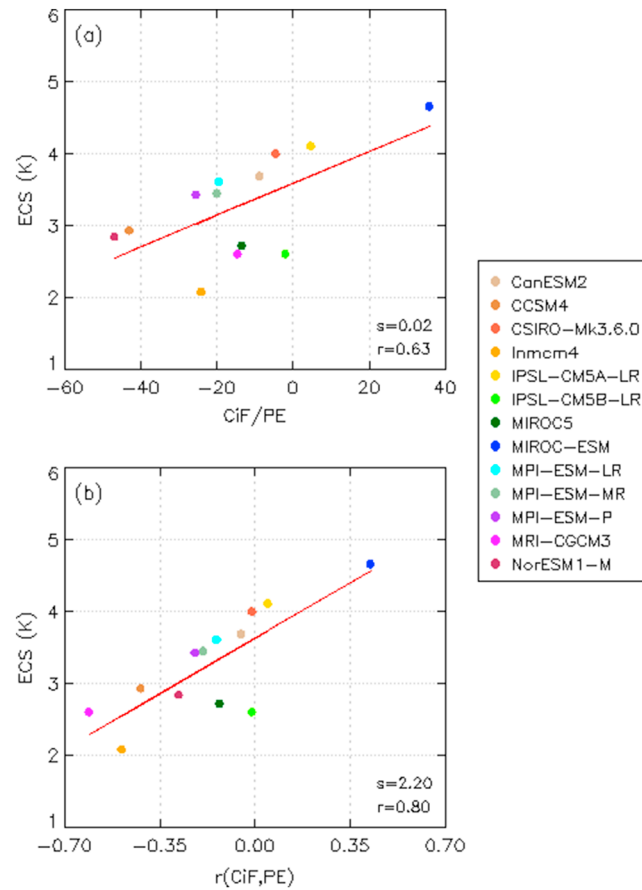
Figure 6. (a) CiF/PE ratio and (b) correlation coefficient between PE and CiF at the 0.1 sigma level against equilibrium climate sensitivity (ECS) of 13 CMIP5 models over the TWP region. At the 0.2 sigma level, such evident relations could not be found. The observed CiF/PE ratio and correlation coefficient between PE and CiF are −104.80 and −0.67, respectively.

not so comparable with those in the models. Rather, in most models, high clouds over the PWP and surrounding areas have often negligible or even strong positive correlations (not shown). This implies that intermodel differences in cloud-precipitation relationships over the domains are quite large. This problem is very likely relevant to the current uncertainty in simulating cloud feedback and climate sensitivity.

It is worth clarifying that this study does not necessarily contradict most of the previous studies concerning the change of total precipitation per se. According to those previous studies, more moisture can be lifted up with intensified convection, moistening the upper atmosphere via the detrainment process [*Sohn et al.*, 2008]. In this process, all types of rain together can increase with the cirrus fraction [*Del Genio and Kovari*, 2002]. In large-scale dynamics, this concept emphasizes the strengthening of the hydrological cycle in a warmer climate. While the global hydrological cycle is strengthened for a warmer climate because of an increase in global precipitation with warming at a rate of about 3% K^{-1}, the tropical circulation as measured by the convective mass flux decreases with the warming. Thus, there is a weakening of the circulation in the tropical Pacific basin [*He and Soden*, 2015; *Held and Soden*, 2006; *Tokinaga et al.*, 2012; *Zhou et al.*, 2011]. In fact, the strength of the hydrological cycle in the tropical Pacific is strongly associated with
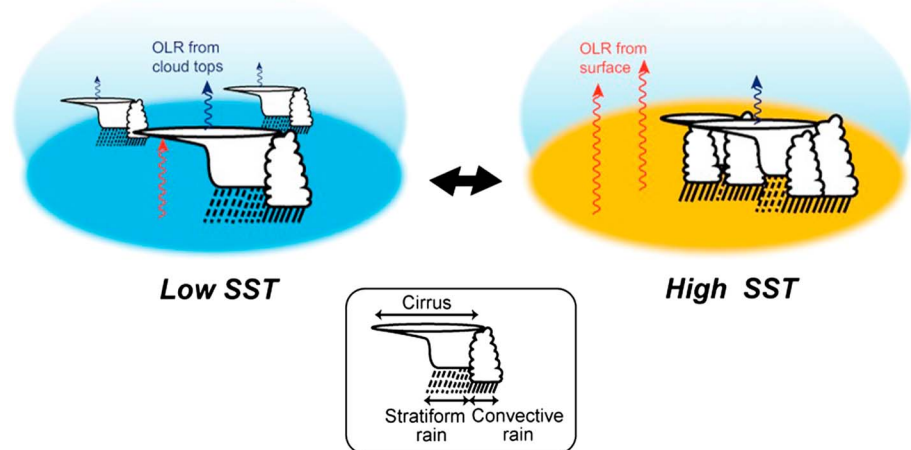
Figure 7. An illustration of the concentration effect of deep convective clouds (DCCs) over the TWP region. Under warmer SST, OLR emission becomes more efficient due to the shrinkage of cirrus fraction per a DCC (the iris effect).

a zonal gradient of SST. This seemingly contradictory relation between precipitation and circulation may be explained by *Su et al.* [2014, 2017] and *Lau and Kim* [2015]. They clearly demonstrated that with more complicated Hadley circulation changes under global warming in the deep tropics, ascending motions are strengthened and narrowed, not weakened.

The large-scale circulations (e.g., Walker and Hadley circulations) are tightly entangled with the convective activity over the western Pacific region, and they are not separate phenomena. When the convective activity over the TWP actively alters the strength of the global circulation, the strength of the Walker (and the Hadley) cell would indeed intensify. On the other hand, if any external forcings (e.g., ENSO) cause the Walker circulation, the convective activity over the western Pacific will also be modulated. In either case, the stronger convection in association with the higher SST anomaly will induce more effective precipitation as a convective rainfall (i.e., more precipitation is allotted to the convective rainfall). This reduces the cirrus per unit mass flux (as measured by precipitation efficiency in this study), and eventually results in negative feedback and strengthens the processes summarized in Figure 7. Such processes in the convectively active region can occasionally expand to other regions, e.g., to the central Pacific as the warm pool expands during El Niño events [*Cai et al.*, 2014] or to the ITCZ following the annual cycle. However, these effects were found to be marginal in our research, and the higher order characteristics needs to be scrutinized elsewhere.

A notable negative relationship between the precipitation efficiency and the cirrus fraction is found in independently retrieved satellite measurements. However, this strong negative relationship is not well represented in our state-of-the-art climate models (Coupled Model Intercomparison Project Phase 5, CMIP5). Given that cirrus clouds are powerful infrared radiative substances, such a misrepresentation would lead to an overestimation of the ECS in the models. In fact, the atmospheric water vapor increase over years closely follows the theoretical Clausius-Clapeyron increase of the moisture contents in the atmosphere (~7% per each degree of warming) [*Held and Soden*, 2006] in the absence of change in the hydrological cycle. When the precipitation efficiency does not constrain the cirrus response, this increase in water vapor as well as the other type of known cloud responses (e.g., the reduction of low cloud fraction and the rise of cloud top height) will exert a strong positive feedback accelerating the temperature response to greenhouse gas forcing. On the other hand, the positive covariance between the SST and precipitation efficiency in the tropics, and their negative correspondence to cirrus clouds, would serve as a strong negative feedback and reduce positive climate feedbacks.

References

Awaka, J., T. Iguchi, and K. Okamoto (2007), Rain type classification algorithm, in *Measuring Precipitation From Space EURAINSAT and the Future*, edited by V. Levizzani et al., pp. 213–224, Springer, Dordrecht, Netherlands.

Behrangi, A., T. Kubar, and B. Lambrigtsen (2012), Phenomenological description of tropical clouds using CloudSat cloud classification, *Mon. Weather Rev.*, *140*(10), 3235–3249.

Bony, S., et al. (2015), Clouds, circulation and climate sensitivity, *Nat. Geosci.*, *8*(4), 261–268, doi:10.1038/ngeo2398.

Bony, S., B. Stevens, D. Coppin, T. Becker, K. A. Reed, A. Voigt, and B. Medeiros (2016), Thermodynamic control of anvil cloud amount, *Proc. Natl. Acad. Sci. U.S.A.*, *113*, 8927–8932, doi:10.1073/pnas.1601472133.

Cai, W., S. Borlace, M. Lengaigne, P. van Rensch, M. Collins, G. Vecchi, A. Timmermann, A. Santoso, M. J. McPhaden, and L. Wu (2014), Increasing frequency of extreme el Niño events due to greenhouse warming, *Nat. Clim. Change*, *4*, 111–116.

CERES Science Team (2013), CERES ES4 Terra Edition3 Data Quality Summary. [Available at https://eosweb.larc.nasa.gov/sites/default/files/project/ceres/quality_summaries/CER_ES4_Terra_Edition3.pdf.]

Chambers, L., B. Lin, and D. Young (2002), Tropical cloud properties from CERES: Does the Iris exist?, paper presented at 34th COSPAR Scientific Assembly.

Cho, H., C.-H. Ho, and Y.-S. Choi (2012), The observed variation in cloud-induced longwave radiation in response to sea surface temperature over the Pacific warm pool from MTSAT-1R imagery, *Geophys. Res. Lett.*, *39*, L18802, doi:10.1029/2012GL052700.

Choi, Y.-S., and C.-H. Ho (2006), Radiative effect of cirrus with different optical properties over the tropics in MODIS and CERES observations, *Geophys. Res. Lett.*, *33*, L21811, doi:10.1029/2006GL027403.

Choi, Y.-S., C.-H. Ho, and C.-H. Sui (2005), Different optical properties of high cloud in GMS and MODIS observations, *Geophys. Res. Lett.*, *32*, L23823, doi:10.1029/2005GL024616.

Choi, Y. S., H. Cho, C. H. Ho, R. S. Lindzen, S. K. Park, and X. Yu (2014), Influence of non-feedback variations of radiation on the determination of climate feedback, *Theor. Appl. Climatol.*, *115*(1–2), 355–364.

Chou, M.-D., and R. S. Lindzen (2002), Comments on "tropical convection and the energy balance at the top of the atmosphere", *J. Clim.*, *15*, 2566–2570.

Chou, M.-D., and R. S. Lindzen (2005), Comments on "Examination of the decadal tropical mean ERBS nonscanner radiation data for the iris hypothesis", *J. Clim.*, *18*, 2123–2127.

Chou, M.-D., R. Lindzen, and A. Hou (2002a), Reply to:" Tropical cirrus and water vapor: An effective earth infrared iris feedback?", *Atmos. Chem. Phys.*, *2*(2), 99–101.

Chou, M.-D., R. S. Lindzen, and A. Y. Hou (2002b), Comments on" The iris hypothesis: A negative or positive cloud feedback?", *J. Clim.*, *15*(18), 2713–2715.

Del Genio, A. D., and W. Kovari (2002), Climatic properties of tropical precipitating convection under varying environmental conditions, *J. Clim.*, *15*(18), 2597–2615.

Fu, Q., M. Baker, and D. L. Hartmann (2002), Tropical cirrus and water vapor: An effective earth infrared iris feedback?, *Atmos. Chem. Phys.*, *2*(1), 31–37.

Graham, N. E., and T. P. Barnett (1987), Sea surface temperature, surface wind divergence, and convection over tropical oceans, *Science*, *238*(4827), 657–659.

Hartmann, D. L., and K. Larson (2002), An important constraint on tropical cloud-climate feedback, *Geophys. Res. Lett.*, *29*(20), 12-11–12-14, doi:10.1029/2002GL015835.

Hartmann, D. L., and M. L. Michelsen (2002a), No evidence for iris, *Bull. Am. Meteorol. Soc.*, *83*(2), 249–254, doi:10.1175/1520-0477(2002)083<0249:NEFI>2.3.CO;2.

Hartmann, D. L., and M. L. Michelsen (2002b), Reply, *Bull. Am. Meteorol. Soc.*, *83*(9), 1349–1352.

He, J., and B. J. Soden (2015), Anthropogenic weakening of the tropical circulation: The relative roles of direct CO_2 forcing and sea surface temperature change, *J. Clim.*, *28*(22), 8728–8742, doi:10.1175/JCLI-D-15-0205.1.

Held, I. M., and B. J. Soden (2006), Robust responses of the hydrological cycle to global warming, *J. Clim.*, *19*(21), 5686–5699, doi:10.1175/JCLI3990.1.

Horváth, Á., and B. J. Soden (2008), Lagrangian diagnostics of tropical deep convection and its effect upon upper-tropospheric humidity, *J. Clim.*, *21*(5), 1013–1028, doi:10.1175/2007jcli1786.1.

Kubar, T. L., D. L. Hartmann, and R. Wood (2007), Radiative and convective driving of tropical high clouds, *J. Clim.*, *20*(22), 5510–5526.

Kubar, T. L., D. E. Waliser, and J.-L. Li (2011), Boundary layer and cloud structure controls on tropical low cloud cover using A-Train satellite data and ECMWF analyses, *J. Clim.*, *24*, 194–215.

Lau, W. K.-M., and K.-M. Kim (2015), Robust Hadley circulation changes and increasing global dryness due to CO_2 warming from CMIP5 model projections, *Proc. Natl. Acad. Sci. U.S.A.*, *112*(12), 3630–3635, doi:10.1073/pnas.1418682112.

L'Ecuyer, T. S., and J. H. Jiang (2010), Touring the atmosphere aboard the A-Train, *Phys. Today*, *63*(7), 36–41.

Lin, B., B. A. Wielicki, L. H. Chambers, Y. Hu, and K.-M. Xu (2002), The iris hypothesis: A negative or positive cloud feedback?, *J. Clim.*, *15*(1), 3–7.

Lin, B., B. A. Wielicki, P. Minnis, L. Chambers, K.-M. Xu, Y. Hu, and A. Fan (2006), The effect of environmental conditions on tropical deep convective systems observed from the TRMM satellite, *J. Clim.*, *19*(22), 5745–5761.

Lin, B., T. Wong, B. A. Wielicki, and Y. Hu (2004), Examination of the decadal tropical mean ERBS nonscanner radiation data for the iris hypothesis, *J. Clim.*, *17*(6), 1239–1246.

Lindzen, R. S., and Y.-S. Choi (2011), On the observational determination of climate sensitivity and its implications, *Asia-Pac. J. Atmos. Sci.*, *47*(4), 377–390, doi:10.1007/s13143-011-0023-x.

Lindzen, R. S., M.-D. Chou, and A. Y. Hou (2001), Does the Earth have an adaptive infrared iris?, *Bull. Am. Meteorol. Soc.*, *82*(3), 417–432, doi:10.1175/1520-0477(2001)082<0417:DTEHAA>2.3.CO;2.

Lindzen, R. S., M.-D. Chou, and A. Y. Hou (2002), Comment on "No evidence for iris", *Bull. Am. Meteorol. Soc.*, *83*(9), 1345–1349, doi:10.1175/1520-0477(2002)083<1345:CONEFI>2.3.CO;2.

Liou, K. N. (1986), Influence of cirrus clouds on weather and climate processes: A global perspective, *Mon. Weather Rev.*, *114*, 1167–1199.

Liu, Z. Y., M. Vaughan, D. Winker, C. Kittaka, B. Getzewich, R. Kuehn, A. Omar, K. Powell, C. Trepte, and C. Hostetler (2009), The CALIPSO Lidar cloud and aerosol discrimination: Version 2 algorithm and initial assessment of performance, *J. Atmos. Oceanic Technol.*, *26*, 1198–1213.

Mauritsen, T., and B. Stevens (2015), Missing iris effect as a possible cause of muted hydrological change and high climate sensitivity in models, *Nat. Geosci.*, *8*(5), 346–351, doi:10.1038/ngeo2414.

Muller, C., and S. Bony (2015), What favors convective aggregation and why?, *Geophys. Res. Lett.*, *42*, 5626–5634, doi:10.1002/2015GL064260.

Ohring, G., B. Wielicki, R. Spencer, B. Emery, and R. Datla (2005), Satellite instrument calibration for measuring global climate change: Report of a workshop, *Bull. Am. Meteorol. Soc.*, *86*(9), 1303–1313, doi:10.1175/BAMS-86-9-1303.

Ramanathan, V., and W. Collins (1991), Thermodynamic regulation of ocean warming by cirrus clouds deduced from observations of the 1987 El Niño, *Nature*, *351*(6321), 27–32.

Rapp, A. D., C. Kummerow, W. Berg, and B. Griffith (2005), An evaluation of the proposed mechanism of the adaptive infrared iris hypothesis using TRMM VIRS and PR measurements, *J. Clim.*, *18*(20), 4185–4194.

Rondanelli, R., and R. S. Lindzen (2008), Observed variations in convective precipitation fraction and stratiform area with sea surface temperature, *J. Geophys. Res.*, *113*, D16119, doi:10.1029/2008JD010064.

Rondanelli, R., and R. S. Lindzen (2010a), Can thin cirrus clouds in the tropics provide a solution to the faint young Sun paradox?, *J. Geophys. Res.*, *115*, D02108, doi:10.1029/2009JD012050.

Rondanelli, R., and R. S. Lindzen (2010b), Comment on "Variations of tropical upper tropospheric clouds with sea surface temperature and implications for radiative effects" by H. Su et al, *J. Geophys. Res.*, *115*, D06202, doi:10.1029/2008JD011189.

Sohn, B. J., J. Schmetz, and E. S. Chung (2008), Moistening processes in the tropical upper troposphere observed from Meteosat measurements, *J. Geophys. Res.*, *113*, D13109, doi:10.1029/2007JD009527.

Sherwood, S. C., S. Bony, and J.-L. Dufresne (2014), Spread in model climate sensitivity traced to atmospheric convective mixing, *Nature*, *505*(7481), 37–42.

Stocker, T., D. Qin, G. Plattner, M. Tignor, S. Allen, J. Boschung, A. Nauels, Y. Xia, B. Bex, and B. Midgley (2013), *Climate Change 2013: The Physical Science Basis. Contribution of Working Group I to the Fifth Assessment Report of the Intergovernmental Panel on Climate Change*, pp. 571–658, Cambridge Univ. Press, Cambridge, U. K., and New York, doi:10.1017/CBO9781107415324.

Su, H., J. H. Jiang, Y. Gu, J. D. Neelin, B. H. Kahn, D. Feldman, Y. L. Yung, J. W. Waters, N. J. Livesey, and M. L. Santee (2008), Variations of tropical upper tropospheric clouds with sea surface temperature and implications for radiative effects, *J. Geophys. Res.*, *113*, D10211, doi:10.1029/2007JD009624.

Su, H., J. H. Jiang, C. Zhai, T. J. Shen, J. D. Neelin, G. L. Stephens, and L. Y. Yung (2014), Weakening and strengthening structures in the Hadley Circulation change under global warming and implications for cloud response and climate sensitivity, *J. Geophys. Res. Atmos.*, *119*, 5787–5805, doi:10.1002/2014JD021642.

Su, H., et al. (2017), Tightening of tropical ascent and high clouds key to precipitation change in a warmer climate, *Nat. Commun.*, *8*, 15771, doi:10.1038/ncomms15771.

Sud, Y. C., G. K. Walker, and K. M. Lau (1999), Mechanisms regulating sea-surface temperatures and deep convection in the tropics, *Geophys. Res. Lett.*, *26*(8), 1019–1022.

Sui, C. H., X. Li, and M. J. Yang (2007), On the definition of precipitation efficiency, *J. Atmos. Sci.*, *64*(12), 4506–4513.

Tokinaga, H., S.-P. Xie, C. Deser, Y. Kosaka, and Y. M. Okumura (2012), Slowdown of the Walker circulation driven by tropical indo-Pacific warming, *Nature*, *491*(7424), 439–443.

Waliser, D. E., and N. E. Graham (1993), Convective cloud systems and warm-pool sea surface temperatures: Coupled interactions and self-regulation, *J. Geophys. Res.*, *98*(D7), 12881–12893.

Wielicki, B. A., B. R. Barkstorm, E. F. Harrison, R. B. Lee III, G. L. Smith, and J. E. Cooper (1996), Clouds and the Earth's Radiant Energy System (CERES): An Earth Observing System Experiment, *Bull. Am. Meteorol. Soc.*, *77*(5), 853–868.

Winker, D. M., W. H. Hunt, and M. J. McGill (2007), Initial performance assessment of CALIOP, *Geophys. Res. Lett.*, *34*, L19803, doi:10.1029/2007GL030135.

Wood, R. (2007), Cancellation of aerosol indirect effects in marine stratocumulus through cloud thinning, *J. Atmos. Sci.*, *64*(7), 2657–2669, doi:10.1175/JAS3942.1.

Zelinka, M. D., and D. L. Hartmann (2010), Why is longwave cloud feedback positive?, *J. Geophys. Res.*, *115*(D16), doi:10.1029/2010JD013817.

Zhang, C. (1993), Large-scale variability of atmospheric deep convection in relation to sea surface temperature in the tropics, *J. Clim.*, *6*, 1898.

Zhou, Y., K. M. Xu, Y. Sud, and A. Betts (2011), Recent trends of the tropical hydrological cycle inferred from Global Precipitation Climatology Project and International Satellite Cloud Climatology Project data, *J. Geophys. Res.*, *116*, D09101, doi:10.1029/2010JD015197.